Synthesis, Characterization, and Li-Electrochemical Performance of Highly Porous Co_3O_4 Powders

G. Binotto,[†] D. Larcher,*[,†] A. S. Prakash,[†] R. Herrera Urbina,[‡] M. S. Hegde,[§] and J-M. Tarascon[†]

Laboratoire de Réactivité et Chimie des Solides, CNRS UMR 6007, 33, rue Saint Leu, Université de Picardie Jules Verne, 80039 Amiens, France, Department of Chemical Engineering and Metallurgy, University of Sonora, Hermosillo, Sonora, Mexico, and Solid State and Structural Chemistry Unit, Indian Institute of Science, Bangalore, India 560 012

Received January 7, 2007. Revised Manuscript Received March 21, 2007

Oxidative precipitation in an aqueous medium of highly self-compacted crystallized Co_3O_4 dense nanoparticles (4−5 nm) leads to the formation of porous micrometric agglomerates exhibiting a well-defined porosity distribution. Postannealing of these powders induces drastic reorganizations first because of the fast removal of trapped water and then because of the particles sintering, resulting in larger interparticle voids. Electrochemical behavior of this nanometric material precipitated at moderate temperature is found to be extremely dependent on the way the mixing with the SP conducting carbon is performed; the better performances being obtained by a soft mixing in an organic solvent. This textural effect provides a stable capacity over the first cycles (800 mA·h/g) and reveals a first cycle capacity loss of the same extent as for bulk Co_3O_4, implying that the nanotexturation undergone by bulk oxide particles during their first formatting cycle is not responsible for the corresponding initial loss. Through chemical analysis of the electrolyte we found that the long-term capacity fading of our materials can be mainly attributed to the dissolution of the active material within the organic electrolyte.

Introduction

Since the demonstration of the Li-ion (rocking-chair) battery feasibility, much research has been focused on the improvement of the anode material performances. Among the numerous explored systems, carbonaceous materials retained much attention because of high reversibility, low cost, no toxicity, and low voltage reaction with metallic lithium. Up to very recently, carbonaceous materials were the only ones implemented in the market despite their limited capacity being a main drawback. This situation changed a few months ago with the commercialization by Sony of Li-ion batteries having an alloy-based material as the negative electrode (Nexelion), leading to much higher gravimetric and volumetric capacities but to a lower long-term reversibility as compared to graphite or related materials. These two examples nicely illustrate the pros and cons of both types of reaction. Alloying reactions, as opposed to intercalation reactions, lead to high capacity but low reversibility. This lack of reversibility has been ascribed for decades to the huge induced volumetric changes associated with phase transitions, and it seems that this problem can be bypassed to some extent by using amorphous or very small metallic particles.[1] In parallel, the possibility of alternative faradic reaction paths prompted intensive research. The chemical and electrochemical Li-reduction of 3d-metal oxides (Mn, Co, Fe) has been thoroughly studied in the 1980s,[2−4] and it was recently demonstrated that bulk particles of transition metal salts MX (M = Co, Cu, Fe, Ni, Ru, ...; X = O, S, N, P, F, ...) electrochemically react with lithium to form composite particles made of amorphous or poorly crystallized Li−X acting as a matrix for nanometric metallic M^0 particles.[5−9] On the basis of a sole transition metal reduction, the global reaction scheme is

$$M^{m+}X_{\frac{m}{x}}^{-} + mLi^0 \rightarrow M^0 + xLi_{m/x}X$$

This first redox reaction therefore comes with a drastic change in the texture of the particles. Whereas their global size and shape is not modified by the reaction, their intimate texture is drastically altered with a transformation of the bulk crystallized initial particles into nanotextured particles made of nanodomains. Down to 0 V vs Li^+/Li^0, note that the first discharge capacity is always found higher than expected for this reaction, because of electrolyte degradation at low voltage and concomitant formation of the decomposition

[†] Université de Picardie Jules Verne.
[‡] University of Sonora.
[§] Indian Institute of Science.

(1) Idota, Y.; Kubota, T.; Matsufuji, A.; Maekawa, Y.; Miyasaka, T. *Science* **1997**, *276*, 1395.
(2) Thackeray, M. M.; Coetzer, J. *Mater. Res. Bull.* **1981**, *16* (5), 591
(3) Thackeray, M. M.; Backer, S. D.; Adendorff, K. T.; Goodenough, J. B. *Solid State Ionics* **1985**, *17* (2), 175.
(4) Thackeray, M. M.; David, W. I. F.; Bruce, P. G.; Goodenough, J. B. *Mater. Res. Bull.* **1983**, *18* (4), 461.
(5) Poizot, P.; Laruelle, S.; Grugeon, S.; Dupont, L.; Tarascon, J. M. *Nature* **2000**, *407*, 496.
(6) Alcántara, R.; Tirado, J. L.; Jumas, J. C.; Monconduit, L.; Olivier-Fourcade, J. *J. Power Sources* **2002**, *109* (2), 308.
(7) Balaya, P.; Li, H.; Kienle, L.; Maier, J. *Adv. Funct. Mater.* **2003**, *13* (8), 621.
(8) Grugeon, S.; Laruelle, S.; Dupont, L.; Tarascon, J.-M. *Solid State Sci.* **2003**, *5*, 895.
(9) Obrovac, M. N.; Dunlap, R. A.; Sanderson, R. J.; Dahn, J. R. *J. Electrochem. Soc.* **2001**, *148* (6) A576.

10.1021/cm070048c CCC: $37.00
Published on Web 05/16/2007

layer at the surface of the reduced particles.[5] Thanks to the as-formed huge Li-X/M^0 internal contact surface, the reduction of the 3d metal was found to be reversible, resulting in reversible storage capacities twice as large as graphite (372 mA·h/g). The nanoscale texture created during the first discharge is maintained during the subsequent sweeps, and the material obtained on top of the charge is thus made of agglomerated nanometric domains of partially recovered MX. Indeed, most of these reactions suffer from large first cycle irreversibility leading to performances that so far do not match the requirements for commercial use. Different origins can be proposed for this loss: partial irreversibility of the electrolyte decomposition occurring at low voltage, loss of active material, and/or not complete back formation of the initial oxide. Several reports indicate that CoO instead of Co_3O_4 is always obtained after one full electrochemical cycle of Co_3O_4/Li cells.[10,11] Most of the first cycle irreversible losses reported in the literature for Co_3O_4 or even Co_3O_4/C composites[5,10−14] match or even exceed the irreversible loss of 2 Li (2 electrons) per formula unit inherent to this Co_3O_4 → CoO transformation. It is thus reasonable to believe that the incomplete back formation upon charge is the main cause of irreversibility of Co_3O_4/Li and other analogous MX/Li cells. Because this capacity loss is taking place during the first textural formatting cycle (nanotexturation), one could logically believe that directly starting from large micrometric agglomerates made of nanometric MX particles (i.e., bypassing the formatting step) could provide a solution to this issue or feed it.

Some nanometric materials, essentially oxides, were found to often exhibit reactivity different from that of the bulk. For instance, alternative reaction paths were found for porous Co_3O_4 vs dense Co_3O_4,[14] for nanotextured vanadium oxide aerogels,[15] and for submicronic hematite compared to bulk α-Fe_2O_3.[16] Above all, it has to be kept in mind that these nanometric powders can exhibit high reversibility versus lithium only when exposed to a limited voltage range. If too low a voltage is applied, such highly divided particles trigger a surface reaction with the electrolytes finally leading to an insulating layer resulting in a loss of electrical connectivity and a capacity fading. Back to our present study, this means that the agglomerates we are willing to prepare have to be as cohesive as possible to limit their destruction along cycling and the formation of surface-reacting individual nanometric particles.

Over the last years, all of these recent findings progressively enlightened the major impact of the different aspects of the powders texture onto their electrochemical reactivity. Because of the ancient belief that only large particles can sustain good reversibility toward lithium, the specific surface area was until recently the only considered textural criterion. Now, all of the other textural aspects have to be thoroughly taken into account: compaction, porous volume, porosity distribution, its evolution upon heating and during electrode processing, and so forth. To simultaneously pay attention to all of these aspects can provide many insights into the powder organization and reactivity, and this is the main point we are addressing in this paper.

Various experimental procedures have been reported in the literature to synthesize nanometric Co_3O_4 particles. Among them, one can quote the oxidative precipitation from aqueous solutions,[17,18] the thermal decomposition of crystallized cobalt alkoxides,[14] inorganic precursors,[19] or polymer fibers,[20] and the elaboration of mesoporous Co_3O_4 by either template removal[21−23] or hydrothermal synthesis.[24,25]

By gathering experimental conditions from different methods, we herein report a simple synthesis procedure to produce micrometric agglomerates made of 4−5 nm Co_3O_4 well-crystallized particles, whose thermal behavior and structural evolution upon postannealing are described. We will show that despite the very small size of the reacting domains, much improved reversibility and good rate capability can be achieved in the 0.01−3.0 V windows provided that great attention is paid to the way the electrode is prepared. Indeed, we will demonstrate that the way the active material is mixed with carbon has a crucial impact on its performances. However, the first cycle capacity loss observed with such preformatted particles is never found lower than with dense bulky oxides, ruling out the responsibility of the initial formatting step onto this electrochemical aspect. Textural evolution during postannealing of this material as well as its dissolution within the battery electrolyte will be discussed.

Experimental Section

Powder Synthesis. Co_3O_4 samples are directly precipitated from a $Co(NO_3)_2$·$6H_2O$ aqueous solution under highly alkaline and oxidizing conditions. In a typical preparation, 22 g of NaOH (550 mmol, Acros, 97%) is dissolved in 800 mL of deionized water in a five-necked flask and heated until boiling under reflux and constant stirring. Once boiling is reached, 16.3 g of $Na_2S_2O_8$ (68.7 mmol, Alfa Aesar, 98%) is dissolved into the solution. Then 50 mL of a 0.69 M $Co(NO_3)_2$·$6H_2O$ solution (10 g, 34.4 mmol, Alfa Aesar, 97.7%) is added dropwise to the previous one, and a black precipitate instantaneously forms. The resulting suspension is aged at 95 °C for 1 h, cooled to room temperature, and left to settle for one night. The black precipitate is separated from the supernatant

(10) Connor, P. A.; Irvine, J. T. S. *Electrochim. Acta* **2002**, *47*, 2885.
(11) Fu, Z.-W.; Wang, Y.; Zhang, Y.; Qin, Q.-Z. *Solid State Ionics* **2004**, *170*, 105.
(12) Needham, S. A.; Wang, G. X.; Konstantinov, K.; Tournayre, Y.; Lao, Z.; Liu, H. K. *Electrochem. Solid-State Lett.* **2006**, *9* (7), A315
(13) Yang, R.; Wang, Z.; Liu, J.; Chen, L. *Electrochem. Solid-State Lett.* **2004**, *7* (12), A496
(14) Larcher, D.; Sudant, G.; Leriche, J.-B.; Chabre Y.; Tarascon, J.-M. *J. Electrochem. Soc.* **2002**, *149*, 234.
(15) Sudant, G.; Baudrin, E.; Dunn B.; Tarascon, J. M. *J. Electrochem. Soc.* **2004**, *151* (5), A666
(16) Larcher, D.; Masquelier, C.; Bonnin, D.; Chabre, Y.; Masson, V.; Leriche J-B.; Tarascon, J.-M. *J. Electrochem. Soc.* **2003**, *150* (1), A133
(17) Sugimoto, T.; Matijevic, E. *J. Inorg. Nucl. Chem.* **1979**, *41* (2), 165.
(18) Xu R.; Zeng, H. C. *J. Phys. Chem. B* **2003**, *107* (4), 926.
(19) Mateos, J. M. J.; Morales, J.; Tirado, J. *J. Solid State Chem.* **1989**, *82* (1), 87
(20) Guan, H.; Shao, C.; Wen, S.; Chen, B. Gong, J.; Yang, X. *Mater. Chem. Phys.* **2003**, *82*, 1002.
(21) Wang, Y.; Yang, C.-M.; Schmidt, W.; Spliethoff, B.; Bill, E.; Schüth, F. *Adv. Mater.* **2004**, *17* (1), 53.
(22) Li, W.Y.; Xu L. N.; Chen, J. *Adv. Funct. Mater.* **2005**, *15*, 851.
(23) Jiao, F.; Shaju K. M.; Bruce, P. G. *Angew. Chem., Int. Ed.* **2005**, *44*, 2−6.
(24) Jiang, Y.; Wu, Y.; Xie, B.; Xie, Y.; Qian, Y. *Mater. Chem. Phys.* **2002**, *74*, 234.
(25) Yang, J.; Quaresma, S.; Mei, S.; Ferreira J. M. F.; Norby, P. *Key Eng. Mater.* **2005**, *280*, 713.

by centrifugation at 3000 rpm for 5 min, washed several times with a 2 M HCl solution to remove byproducts such as β-CoOOH (Heterogenite-3R), washed with water to eliminate residual chlorine, and dried at 50 °C for 12 h. This As-Prepared product will be now referred to as Co_3O_4-AP. Equal amounts (ca. 200 mg) of Co_3O_4-AP are heated under air (5 °C/min) at temperatures ranging from 200 °C to 800 °C and maintained at the required temperature for 1 h. These samples are labeled $Co_3O_{4\ T°C}$ ($Co_3O_{4\ 200°C}$, ..., $Co_3O_{4\ 800°C}$). A batch of β-CoOOH was prepared at ambient temperature by slowly dropping 40 mL of an aqueous hydrogen peroxide solution (110 volumes) into the alkaline solution of cobalt nitrate.

Powder Characterization. X-ray diffraction (XRD) data were collected with an Inel CP120 (Cr Kα, $\lambda = 2.2897$ Å, Al holder) and a D8 Bruker-AXS (PSD detector, Co Kα, $\lambda = 1.79026$ Å, glass holder) diffractometers. The crystallite size was calculated using the Williamson−Hall method[26] from the width of the (111), (220), (311), (400), and (440) peaks. The instrumental broadening was subtracted assuming Gaussian profiles ($\beta_{obs}^2 = \beta_{cryst}^2 + \beta_{instr}^2$). Thermogravimetric analysis (TGA) data were collected either under static air (Mettler M3-TC11) or under Ar/H_2 (5 wt %, Carburos Metálicos) flow (Perkin-Elmer TGA7) in an open alumina crucible. All data were corrected for the variations of the buoyancy of the sample container itself. Infrared spectra were obtained with a Nicolet Avatar 370 DTGS spectrometer in transmission mode between 4000 cm^{-1} and 400 cm^{-1}. Transparent pellets were prepared by pressing a (8 t/cm^2), dispersion of powders in KBr kept at 125 °C. Specific surface areas and pore size/volume distribution were computed from the results of N_2 physisorption at 77 K (Micromeritics ASAP 2020) using the BET (Brunauer−Emmet−Teller)[27] and BJH (Barrett−Joyner−Halenda)[28] formalisms, respectively. The samples were initially outgassed under 30 μm Hg at 120 °C for 4 h. The porous volume was computed to express the agglomerates packing as follows: % porosity = (porous volume)/(porous volume + solid volume). So, 50% porosity describes agglomerates with a porous volume equal to the volume filled by the matter. Assuming dense particles, the specific volume they fill is given by 1/density.

The powder textural/structural study was completed using a high-resolution transmission electron microscope (Philips Tecnaï 200 F20) operating at 200 kV. A suspension of the powder in acetone was energetically dispersed in an ultrasonic bath, and a drop of this well-dispersed suspension was then deposited on a piece of 200-mesh holey carbon-coated copper grid. Particle morphology was also checked by scanning electron microscopy (SEM, Quanta 200F FEG) equipped with a Link-Isis Oxford EDS (electron dispersive spectroscopy) probe.

The cobalt mean oxidation state has been measured by iodometric titration. For such analysis, the powdered sample had to be dissolved in a boiling hydrochloric acid (6 M) solution containing a large excess of dissolved KI and under constant and vigorous N_2 flow. Back to room temperature, I_2 resulting from the oxidation of iodide by Co^{3+} ($E^0(Co^{3+}/Co^{2+}) = 1.92$ V vs SHE) was quantified by hyposulfite titration with soluble starch as the end-reaction indicator. The total amount of cobalt in the initial batch (i.e., total Co^{2+} amount in the final solution) was then evaluated by EDTA (ethylenediaminetetraacetic acid) titration. This method was validated by analysis of Co^{II} and Co^{III} powders (β-CoOOH and $CoCl_2 \cdot 6H_2O$) showing an accuracy of ±1%. The total cobalt amount was confirmed for some samples by a direct cobalt determination through atomic absorption analysis (Perkin-Elmer AAnalyst 300).

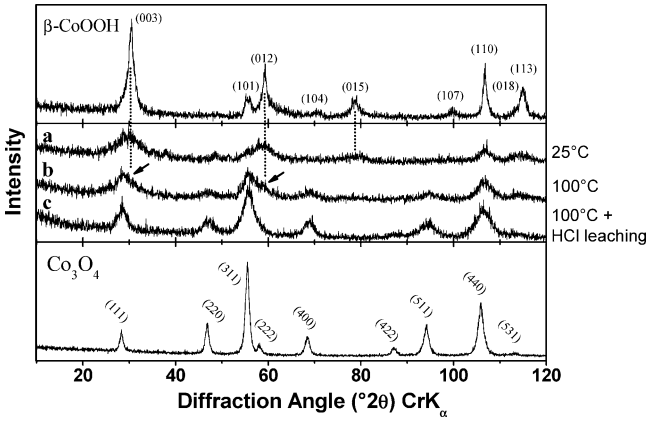

Figure 1. XRD patterns (Cr Kα, $\lambda = 2.2897$ Å) for the precipitates obtained at 25 °C (a), 100 °C (b), and after HCl leaching of the powder precipitated at 100 °C, labeled as Co_3O_4-AP (c). See experimental procedure for more details. XRD patterns for bulk Co_3O_4 and for β-CoOOH are given for reference in the bottom and top panels, respectively.

Analysis of gas released during annealing of Co_3O_4-AP and CoOOH was achieved by a mass spectrometer (Netzsch QMS 403 Aeolos) coupled with a thermo-balance (Netzsch STA 449 Jupiter) operating under primary vacuum.

Typically, positive electrodes were prepared by hand-mixing 80 wt % of active material with 20 wt % SP carbon, as the electronic conductor, using a pestle and mortar, and for a 10−15 min period. As a result of their high specific surface area, these powders are prone to pick up air moisture, the reason why they were kept in a drying oven at 100 °C for 12 h before mixing. Details on the mixing step, which turns out to strongly affect the electrochemical performances, will be given throughout the paper. Once the electrode was prepared, Swagelok cells were assembled in an argon filled glovebox with about 5−8 mg of the mix separated from the lithium foil by two sheets of Whatman glass fiber disks, all of it being soaked in a 1 M $LiPF_6$ solution in an ethylene carbonate (EC)/dimethyl carbonate (DMC) mixture (1:1, v/v). Typically, galvanostatic tests were conducted between 3.0 and 0.01 V at constant temperature (25 °C) with a Mac Pile controller at a Q/5 charge−discharge rate (1 Li per formula unit in 5 h).

The rate capability of the samples ("signature curve") was obtained as proposed in ref 29. In a typical test, the cell is discharged to 0.01 V vs Li^+/Li^0 at a current rate of $Q/5$ to determine the initial full cell capacity. Then the cell is first charged at a high rate of $4Q$ up to a charge cutoff potential of 3 V vs Li^+/Li^0 and left in an open circuit potential for 30 min. The same sequence is then repeated with progressively lowering the current/rate, the overall capacity being obtained by cumulating the capacity for each step.

The level of dissolution of the active material in the electrolyte was determined after soaking for one month, at 25 °C, and under argon, 6.8 mg of oxide in 0.6 mL of electrolyte ($LiPF_6$/EC/DMC). Then, 0.1 mL of the supernatant was dropped in 100 mL of deionized water and analyzed by atomic absorption spectroscopy.

Results and Discussions

Synthesis and Characterization of Co_3O_4-AP. XRD patterns displayed in Figure 1 show that the phase composition of the recovered powder prior to the HCl washing step is highly dependent on the precipitation temperature. Although the Bragg reflections are very broad, a first indication of small and/or poorly crystallized domains, the formation

(26) Williamson, G. K.; Hall, W. H. *Acta Metall.* **1953**, *1*, 22.
(27) Brunauer, S.; Emmet P. H.; Teller, E. *J. Am. Chem. Soc.* **1938**, *60*, 309.
(28) Barrett, E.; Joyner, L.; Halenda, P. *J. Am. Chem. Soc.* **1951**, *73*, 373.
(29) Doyle, M.; Newman, J.; Reimers, J. A. *J. Power Sources* **1994**, *52*, 211.

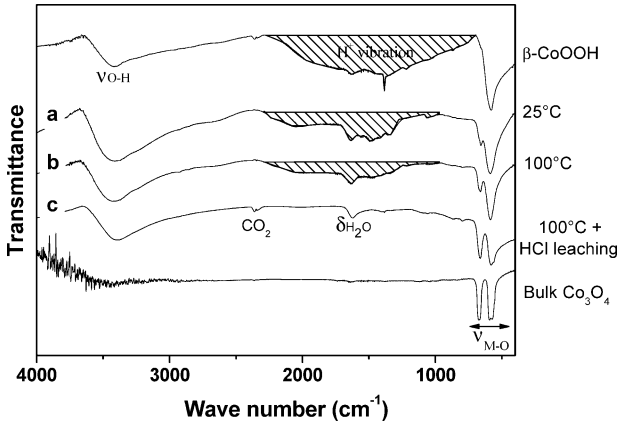

Figure 2. Infrared spectra of the precipitates obtained at 25 °C (a), 100 °C (b), and after HCl leaching of the powder precipitated at 100 °C, labeled as Co_3O_4-AP (c). The spectra for bulk Co_3O_4 and for β-CoOOH are given for reference in the bottom and top panels, respectively.

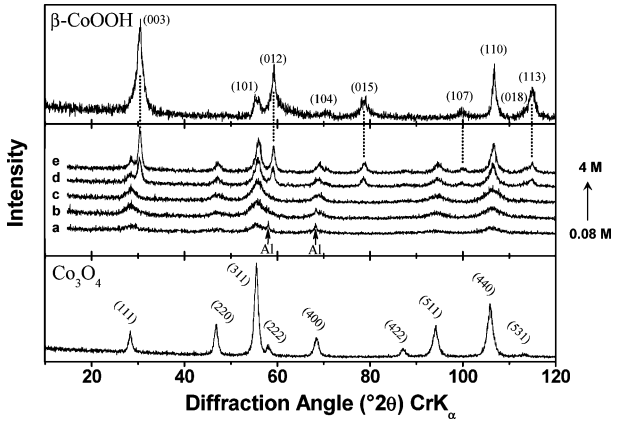

Figure 3. Evolution in powder XRD patterns (Cr Kα, $\lambda = 2.2897$ Å) as a function of the Co nitrate concentration, ranging from 0.08 M (a) to 4 M (e). The XRD patterns for bulk Co_3O_4 and for β-CoOOH are given for reference in the bottom and top panels, respectively.

of β-CoOOH (Heterogenite-3R) appears to be favored at low temperature (Figure 1a**)**, while higher temperature facilitates that of the spinel phase (Figure 1b). Nevertheless, even when working at the boiling point, β-CoOOH can be guessed together with Co_3O_4. This is better shown from infrared data (Figure 2). Aside from characteristic signals of H_2O (1630 cm^{-1}), vibrations of Co ions in octahedral sites (ν_1, 586 cm^{-1}, and ν_2, 658 cm^{-1}),[30] OH (broad band centered at 3400 cm^{-1}), and CO_2 (doublet at 2300 cm^{-1}), a broad and diffuse absorption band spreads from 2500 to at most 1000 cm^{-1} and is related to the H^+ vibration within the β-CoOOH interlayer space.[31] As suspected from Figure 1, the intensity of this band is indeed slightly but visibly lowered going from ambient temperature to the boiling point. $T = 100$ °C was then selected as the optimized temperature, but the unavoidable CoOOH impurity had to be leached out anyway. Keeping in mind that CoOOH is much more soluble than Co_3O_4 in acid media, this was nicely achieved by HCl treatments,[17] as indicated by the absence of both the XRD peak shoulder (Figure 1c) and the diffuse infrared band (Figure 2c). The air-annealing of CoOOH at about 300 °C is well-known to give Co_3O_4,[32,33] but in our case we prefer the HCl treatment to preserve the low-temperature texture.

The infrared M-O signal witnesses a progressive splitting and an increasing relative intensity of the ν_2 band when one uses higher temperature and after acid washing. Also worth pointing out is the very large intensity of the hydroxyl ν-OH stretching band with respect to the water δ-H_2O bending vibration. This means that our Co_3O_4-AP powder contains a large amount of OH groups, mainly unrelated to adsorbed water. The presence of (oxi)hydroxides being hardly believable subsequently to the acidic leaching, it suggests a highly divided material with OH-covered surface, as will be confirmed later. Finally, the main features of both the XRD pattern and the infrared spectrum of Co_3O_4-AP are well matching those of pure spinel. However, a careful examination reveals that the relative intensities of the (111) and (220) Bragg peaks are not matching those expected for such a normal spinel structure. This point is presently under consideration and will be the topic of a forthcoming paper.

Although the intimate mechanism linked to the competing precipitations of CoOOH and Co_3O_4 is not yet fully understood, controlling the amount of CoOOH by varying the cobalt concentration in the precipitation medium was not successful. It turned out that increasing the Co concentration resulted in a higher powder yield and CoOOH content (Figure 3). The amount of oxidizing agent being kept constant, this result confirms the role of the nitrate ions. Lowering the concentration was logically found to limit the yield of the reaction but does not significantly affect the CoOOH proportion.

The broadness of the XRD peaks (Figure 1) prevents any accurate determination of the cubic cell parameter ($a \sim 8.09$ Å), but it can be used to evaluate the crystallite size of Co_3O_4-AP to be 4−5 nm and isotropic. Transmission electron microscopy (TEM) pictures (Figure 4a) reveal well-crystallized Co_3O_4 particles of this exact size, with a very narrow size distribution and that are highly agglomerated. Thus, each particle is a crystallite, a monolithic domain. The size of the agglomerates was found by SEM to be between 1 and 10 μm (Figure 4b), each agglomerate being therefore made of several billions of nanoparticles. The amount of residual Na coming from $Na_2S_2O_8$ and NaOH reagents was found by EDS analyses, performed on large areas, to be lower than the resolution limit of our apparatus (1%). The high BET specific surface area calculated from data of N_2 adsorption (230 m^2/g) is in perfect agreement with the theoretical value calculated assuming dense and homogeneous Co_3O_4 spheres ($\rho = 6$ g/cm^3) with diameters ranging from 4 nm (250 m^2/g) to 5 nm (200 m^2/g). This is an important indication of the absence of intra-particle porosity. However, both the large hysteresis in the N_2 isotherm adsorption/desorption curve and the pore size distribution (Figure 5) demonstrate a high interparticle mesoporosity with a narrow porous volume distribution of about 4 nm in pore size and no significant porosity for pores larger than 6 nm (inset, Figure 5). The shape of the isotherm curve (IVa type) is well-described in the literature as a result of a network of bottleneck interconnected

(30) Nkeng, P.; Poillerat, G.; Koenig, J.-F.; Chartier, P.; Lefez, B.; Lopitaux, J.; Lenglet, M. *J. Electrochem. Soc.* **1995**, *142* (6), 1777
(31) Delaplane, R. G.; Ibers, J. A.; Ferraro, J. R.; Rush, J. J. *J. Chem. Phys.* **1969**, *50* (5), 1920.
(32) Avramov, L. K. *Thermochim. Acta* **1974**, *10*, 409.
(33) O'Brien, P.; Patel, U. *J. Chem. Soc., Dalton Trans* **1982**, *8*, 1407.

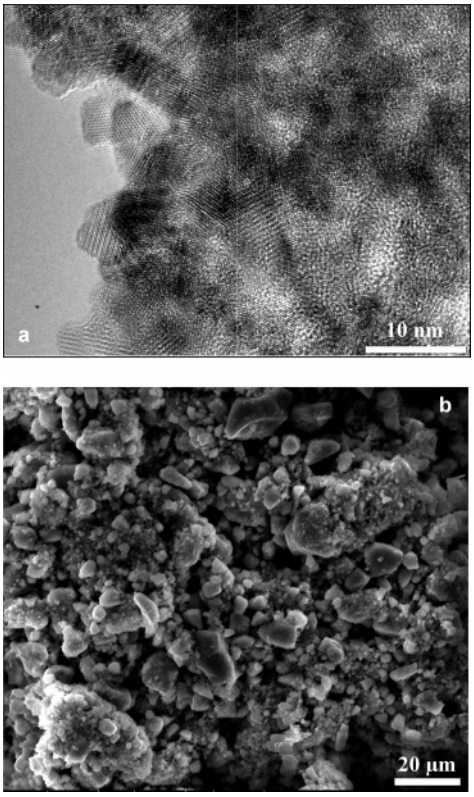

Figure 4. Electron microscopy images for Co_3O_4-AP showing the nanoparticles (a, TEM) and the agglomerates of these nanoparticles (b, SEM)

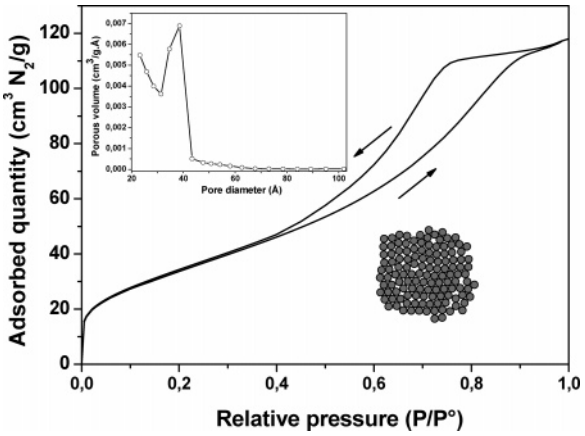

Figure 5. Nitrogen adsorption/desorption isotherm (77 K) curve for Co_3O_4-AP and porous volume distribution as a function of pore size computed with the BJH method (inset). Prior to analysis, samples were treated at 30 μm Hg and 120 °C for 4 h. Schematization of the intimate organization of the Co_3O_4-AP powder is also shown.

pores.[34] Indeed, the equivalent size of the particles and of the pores resulting from their agglomeration implies high packing, as confirmed by the porous volume contribution (42%), meaning 58% of the available volume filled by the particles. On the basis of a hard sphere model, this last value lies between that of a primitive cubic (52%) and that of a body-centered cubic packing (68%). It has to be kept in mind that this porosity contribution can be seen as a packing indicator. Thus, our powders are made of large and porous agglomerates consisting of highly packed, dense, and nonporous nanoparticles. Whatever the reaction time, bath temperature, or Co nitrate concentration, no significant modification in the nanoparticles size, surface area, or packing could be evidenced.

(34) Gregg J.; Sing, K. S. W. *Adsorption, Surface Area and Porosity*; Academic Press: New York, 1982.

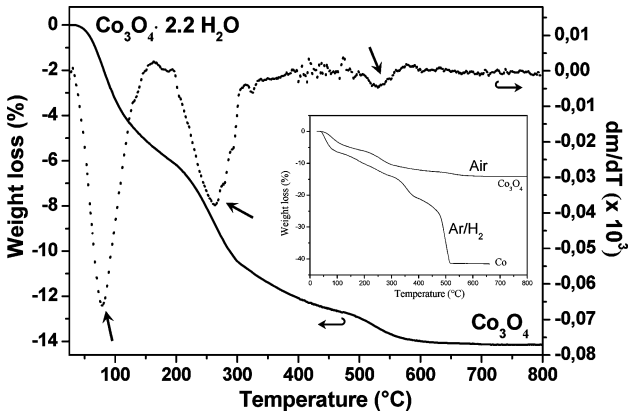

Figure 6. TGA curve (air, 5°/min) for Co_3O_4-AP and derivative $\partial m/\partial T$ plot (dashed). Inset: comparison between weight losses measured under air and under Ar/H_2 (5%) flow.

From the mean cobalt oxidation state (2.66 ± 0.03), the cobalt content as deduced from atomic absorption (85%), and the large amount of surface hydroxyl groups evidenced by infrared spectroscopy, one can suggest $Co_3O_4 \cdot 2.2H_2O$ as the formula for Co_3O_4-AP.

Thermal Behavior of Co_3O_4-AP. The heating of Co_3O_4-AP up to 800 °C under air comes with three distinct losses, identified as water losses by mass spectrometer analysis (not shown here), and this overall weight evolution (14%) confirms the formula $Co_3O_4 \cdot 2.2H_2O$. These losses are centered at 70 °C (surface water), 250 °C (trapped water), and 500 °C (hydroxyl groups), respectively (Figure 6). The same set of treatment/analysis applied to CoOOH revealed water and O_2 releases consequently to the cobalt reduction ($6CoOOH \rightarrow 2Co_3O_4 + {}^1/_2O_2 + 3H_2O$). The absence of such O_2 release for Co_3O_4-AP further confirms the efficiency of the acidic leaching in dissolving the oxy-hydroxide byproduct. Aside from very small CO_2 and Cl_2 signals (<1%), no other gaseous annealing products were detected. Thermogravimetric analyses performed under reducing Ar/H_2 (5%) flow led to metallic cobalt (inset, Figure 6) with a global weight loss corresponding to the same chemical formula for Co_3O_4-AP. The analysis of this TGA curve reveals different reduction steps, suggesting a potential catalytic activity for this material. This will be the subject of a forthcoming paper.

Evolution in XRD patterns for $Co_3O_{4\ T°C}$ is depicted in Figure 7. From these patterns we could calculate the evolution in crystallite size as a function of T (Figure 7b). The parallel evolutions in BET value, porosity contribution (%), and porous volume distribution are shown on Figure 8. As expected, the crystallite size increases with the annealing temperature. Except for $Co_3O_{4\ 800°C}$, the geometric specific surface areas calculated from the crystallite sizes (Figure 7b) always match the values obtained from N_2 adsorption (Figure 8), ruling out the creation of large intra-particle porosity. For $Co_3O_{4\ 800°C}$, the much smaller measured BET value (1 m^2/g) than the calculated one (16 m^2/g) indicates coarsening and formation of large mosaic particles. Because our samples were systematically heated under low pressure at 120 °C before porosity measurements, one can consider that the

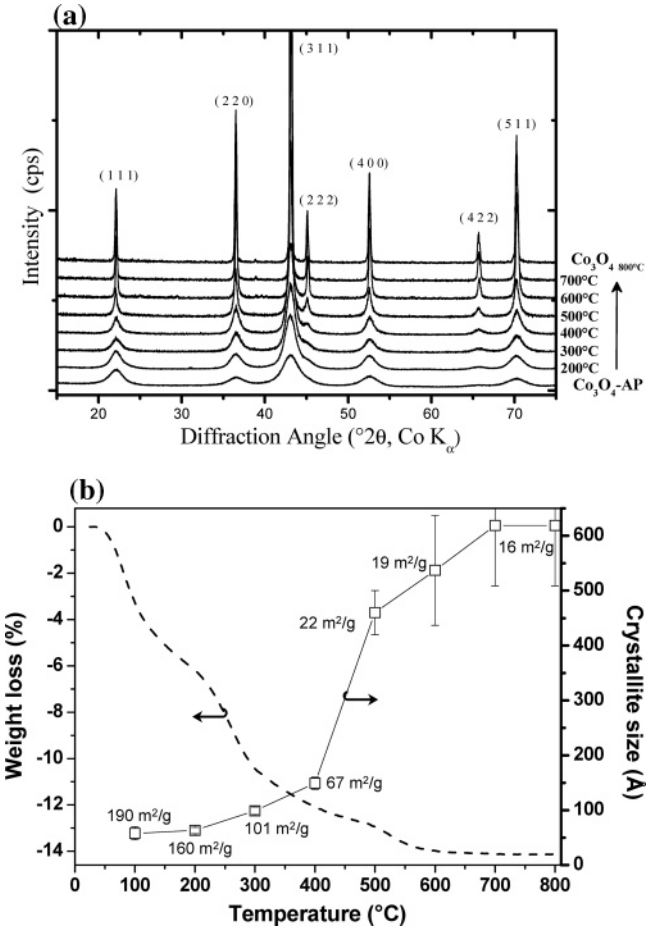

Figure 7. Evolution of XRD patterns for Co_3O_4-AP and Co_3O_4 $_{T\ °C}$ as a function of T (a) and related evolution of crystallite size (b). The TGA curve performed under air is superimposed (dashed line). Geometric specific surface area values are those calculated from the crystallite sizes.

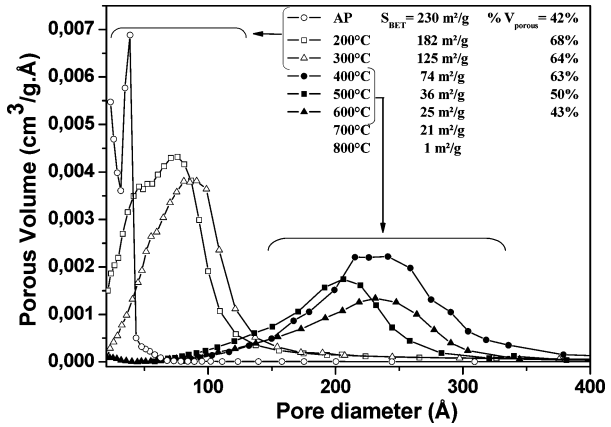

Figure 8. Porous volume distribution as a function of the pore size for Co_3O_4-AP and Co_3O_4 $_{T\ °C}$. BET values and porous volume proportions are also given.

loosely bonded water (first water loss) is already gone. Heating at higher temperature (200 °C) induces a large increase in porosity (42% → 68%) while the BET specific surface area is only slightly lowered as a result of a limited coarsening at such low temperature. At the same time, we observe an important broadening of the porous volume distribution up to 100 Å in pore diameter (Figure 8). These modifications can be figured out assuming a disorganization of the agglomerates as a result of the fast expulsion of a large amount of trapped and over-heated water, leading to a looser compaction and larger inter-particles voids. Above 200 °C, the porous volume then gradually drops as the specific surface area does. The sharp rise in crystallite size occurring between 400 °C and 600 °C is concomitant with the departure of surface hydroxyl groups. This last point can easily be understood if one considers that the coarsening of such small particles results in a large drop in the specific surface area, itself resulting in a release of large amounts of hydroxyl surface-covering groups. From another point of view, one can consider that coarsening is prevented as long as surface groups are screening the particles.

Accordingly, the maximum in the porous volume as a function of the pores diameter drastically shifts from 100 Å ($T \leq 300$ °C) to around 200−250 Å ($T \geq 400$ °C). Porosity is no longer detected for T ≥ 700 °C, and the TEM images of Co_3O_4 $_{800°C}$ show well crystallized particles with sizes ranging from 500 to 3000 Å.

Electrochemical Behavior of Co_3O_4-AP and Annealed Samples. Because it is used as a conducting additive in our electrodes (20 wt %), SP carbon deserves its own characterization. It consists of 50 nm spherical particles (Figure 9a) with a S_{BET} of 55 m^2/g and no significant porosity (Figure 9b) compared to Co_3O_4-AP. It reacts with Li^0 exchanging about 420 mA·h/g during the first discharge step, and about 200 mA·h/g reversibly in the 3.0−0.0 V range vs Li^+/Li^0 (Figure 9c). Owing to the small contribution of SP carbon onto the overall capacity (more than 1100 mA·h/g), it will be neglected so that capacities of all Co_3O_4-based electrodes will be given as mA·h/g of Co_3O_4.

Co_3O_4-AP/SP and Co_3O_4 $_{800°C}$/SP hand-mixed powders were found to react with lithium (1 Li/5 h) in very different ways (Figure 10). The first discharge is much longer for Co_3O_4-AP (1400 mA·h/g) than for Co_3O_4 $_{800°C}$ (1150 mA·h/g), with somewhat a similar first cycle irreversible loss (400−450 mA·h/g). In contrast, capacity rapidly fades for Co_3O_4-AP while 600 mA·h/g can be maintained for at least 30 cycles with Co_3O_4 $_{800°C}$. This much larger first discharge capacity is consistent with a much higher surface area accessible to the electrolyte and thus to its enhanced electrochemical degradation. Keeping in mind that the intimate texture of Co_3O_4-AP mimics that of Co_3O_4 $_{800°C}$ after the first formatting cycle, they should exhibit similar behavior. At this point, one can therefore wonder whether the commonly used way of mixing active material with SP can be responsible for such behavior.

To ensure this point, we first ground Co_3O_4-AP without SP using the same method and milling time as applied for electrodes making. Although the XRD pattern and infrared spectrum were not altered, this milling caused an important increase in porous volume (42% → 53%) and a drastic widening of the porous distribution with smaller intensity of the 4 nm peak for the benefit of higher pore size (Figure 11). These data suggest an intense breaking of the agglomerates and the creation of large inter-agglomerates pores, as schematized in Figure 11. Similar porosity tests onto the hand-milled Co_3O_4-AP/SP mixture still exhibit a downsized 4 nm contribution (i.e., smaller agglomerates) but with an almost complete vanishing of the large pores contribution. The broad porous distribution is no longer present, and we

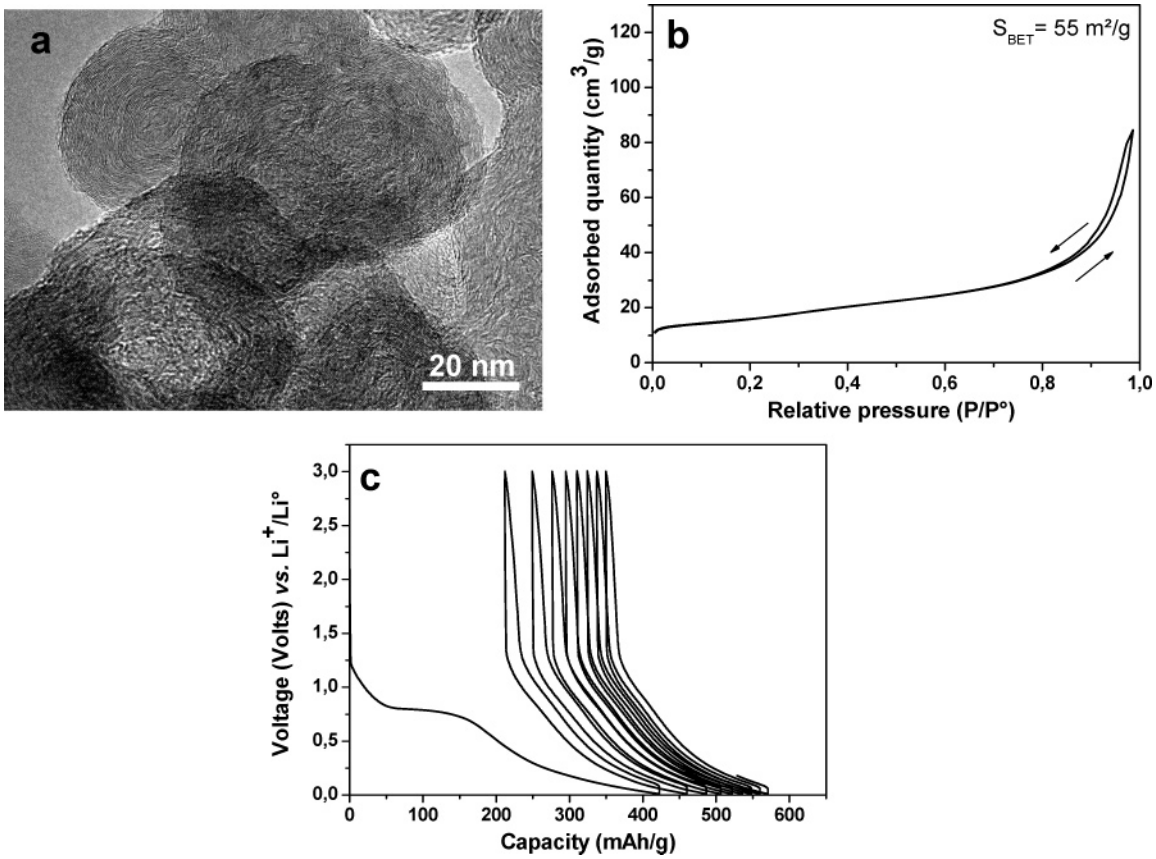

Figure 9. Characterization of SP carbon: TEM images (a), N_2 adsorption/desorption isotherm (77 K) curve (b), and electrochemical galvanostatic activity vs metallic lithium (rate *Q*/10, 20 °C; c).

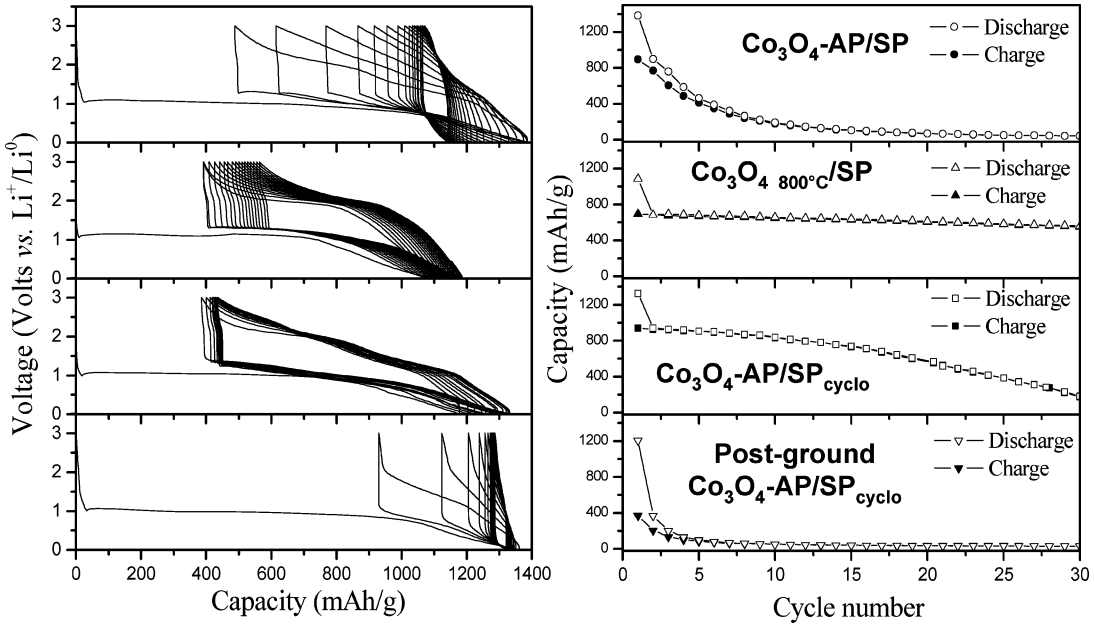

Figure 10. Galvanostatic cycling (1 Li/5 h, 20 °C; left panels) and charge/discharge capacities as a function of cycle number (right panels) for Co_3O_4-AP/SP, $Co_3O_{4\ 800°C}$/SP, Co_3O_4-AP/SP_{cyclo}, and post-ground Co_3O_4-AP/SP_{cyclo}.

believe this is due to the filling of the inter-agglomerates porosity with the SP particles. Despite this apparent narrow pore distribution, the breaking of the agglomerates leads to higher accessibility of the electrolyte toward the surface of the oxide nanoparticles, consistent with the very bad electrochemical cycling vs Li^0 for Co_3O_4-AP/SP.

After many unsuccessful attempts systematically resulting in a bad compromise between good mixing and minimization of the agglomerates breaking, another approach was tested.[15] Without any preliminary hand-mixing, we suspended 50−70 mg of Co_3O_4-AP plus 20 wt % of SP in 60 mL of cyclohexane. As a result of both toxicity and volatility of this solvent, all steps were done an under air-extracted fume hood. The suspension was magnetically stirred during 30 min at ambient temperature under air. The powder was then left to decant, the supernatant was progressively pumped out,

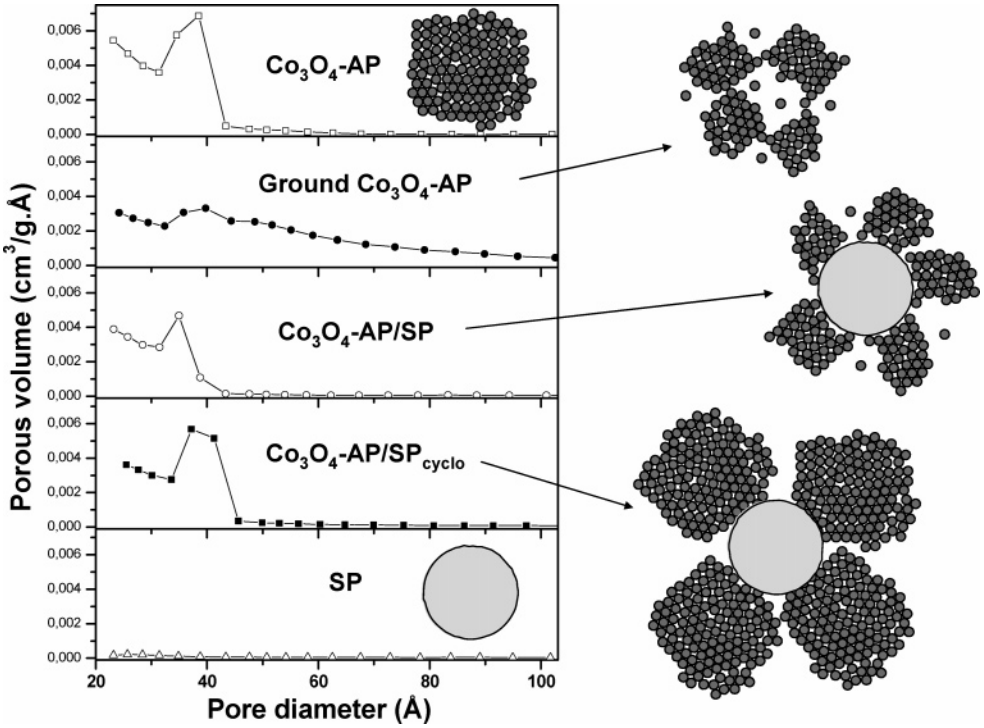

Figure 11. Porous volume distribution as a function of the pore size for Co_3O_4-AP, ground Co_3O_4-AP, Co_3O_4-AP/SP, Co_3O_4-AP/SP_{cyclo}, and SP carbon.

and the dry powder was finally recovered after overnight self-evaporation of the remaining solvent. The so-obtained powder is labeled as Co_3O_4-AP/SP_{cyclo}. After a similar cyclohexane treatment performed on Co_3O_4-AP alone, we checked by XRD, N_2 adsorption, infrared and atomic absorption spectroscopy that it affects neither the chemical composition, the structure, nor the texture of the powder. The complete evaporation of cyclohexane was checked by infrared spectroscopy (i.e., no C−H stretching bands), and possible oxide dissolution was ruled out by atomic absorption analysis of the supernatant. Porosity distribution and porous volume were found to be much less altered for Co_3O_4-AP/SP_{cyclo} than for Co_3O_4-AP/SP (Figure 11) indicating a much milder way of mixing powders, as well as limited breaks of the agglomerates and limited creation of wide porosity. In addition, porosity results are now rather close to the theoretical ones obtained by considering the addition of 20 wt % of nonporous SP powder. TEM pictures illustrated and visually confirmed the differences between Co_3O_4-AP/SP_{cyclo} and Co_3O_4-AP/SP with large agglomerates (dense zones) for the former and pulverized agglomerates for the latter (Figure 12).

According to their similar specific surface area, Co_3O_4-AP/SP_{cyclo} and Co_3O_4-AP/SP have almost identical (1330−1380 mA·h/g) first discharge capacities (Figure 10). Thanks to the mixing method, the cycling stability is now well improved. For instance, 800 mA·h/g is still reached for Co_3O_4-AP/SP_{cyclo} after 15 cycles, compared to no more than 100 mA·h/g for Co_3O_4-AP/SP. This mixing effect was further demonstrated by the lack of reversibility shown by a post-ground Co_3O_4-AP/SP_{cyclo} batch (Figure 10).

It is now well-established that the first reaction step with lithium of small Co_3O_4 domains is the formation of a mixture of Li_2O and CoO, whereas large crystallites are undergoing reduction by Li insertion in the spinel structure.[3,14] This

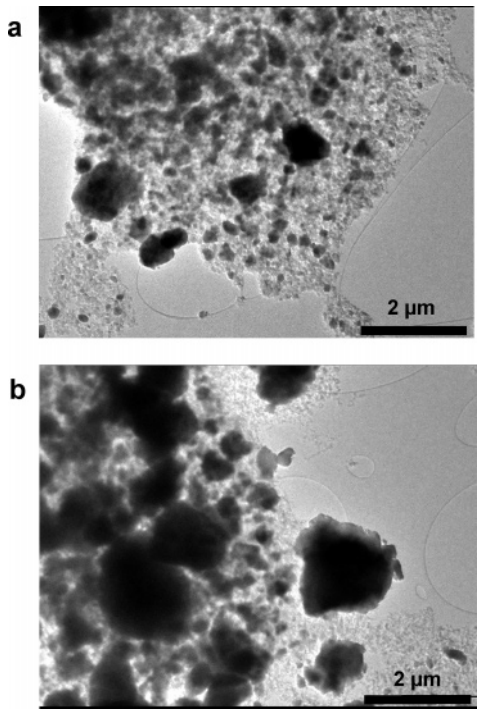

Figure 12. TEM pictures for Co_3O_4-AP/SP (hand-mixing; a) and for Co_3O_4-AP/SP_{cyclo} (mixing in suspension in cyclohexane; b). Note the very smaller size of the agglomerates for Co_3O_4-AP/SP compared to Co_3O_4-AP/SP_{cyclo}.

drastic difference between large and small reacting domains can be used to provide an additional demonstration of the bypass of the initial formatting step. Indeed, we could observe, by in situ X-ray experiments (not shown here) collected during the cycling of cells containing Co_3O_4-AP/SP_{cyclo} and $Co_3O_{4\ 800°C}$/SP electrodes, that the first reduction of Co_3O_4-AP comes, as expected, with the formation of CoO. In contrast, this is only observed during the second reduction of $Co_3O_{4\ 800°C}$, the first one leading to inserted $Li_xCo_3O_4$.

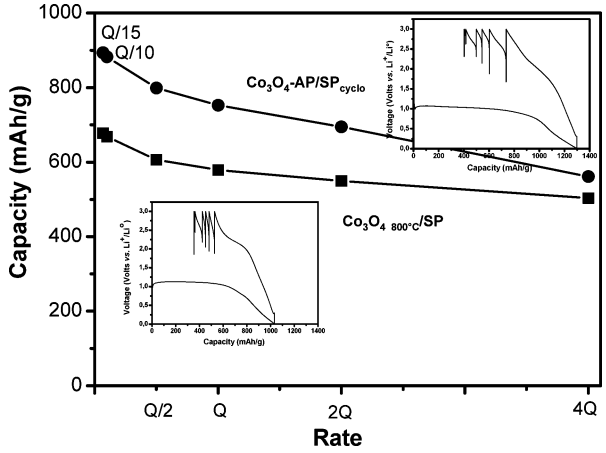

Figure 13. Compared charge capacities as a function of the rate (Q/x = one Li in x h) for Co_3O_4-AP/SP_{cyclo} and Co_3O_4 800°C/SP electrodes (20 °C). Insets: corresponding galvanostatic voltage vs composition plots.

Besides different internal organization (porous agglomerates vs dense particles), a Co_3O_4-AP/SP_{cyclo} electrode appears very similar to a Co_3O_4 800°C/SP mix, and then should behave similarly. However, long-term cycling of Co_3O_4-AP/SP_{cyclo} proves a progressive fading, not yet fully understood, but we cannot discard a possible electrochemical grinding leading to a progressive pulverization of the agglomerates. TEM and SEM surveys are underway to address this point.

Dissolution of the active material was at first sight ruled out by the absence of a Co-containing deposit at the surface of the Li foil, at least within the detection limit of our device (1%). These EDS analyses were performed on Li disks washed several time with salt-free electrolyte and after 30 cycles. However, after soaking for one month a batch of Co_3O_4-AP/SP at ambient temperature in the electrolyte ($LiPF_6$/EC/DMC), we detected by atomic absorption an important dissolution of the oxide (22%). The intense coloration of the electrolyte suggests the formation of stable solvated Co species that could explain the absence of large deposits onto the Li foil. Even more interesting is that similar experiments conducted on Co_3O_4-AP/SP_{cyclo} (12% dissolution) and Co_3O_4 800°C (0.7% dissolution) revealed a trend between the long-term cycling efficiency (Figure 10) and the extent of dissolution in the electrolyte. We thus believe this dissolution is a key point to be tackled in view of optimization of such powders, and we are presently coating them with ionic/electronic conductors.

Despite this tendency to dissolution and that the rate capability for Co_3O_4-AP/SP_{cyclo} well compares to that of Co_3O_4 800°C/SP, the electrode can sustain high rates with charge capacity dropping from 900 mA·h/g at Q/15 to 600 mA·h/g at 4Q (Figure 13).

Aside from long-term cycling and rate capability, it is important to observe that Co_3O_4-AP/SP_{cyclo} and Co_3O_4 800°C/SP exhibit exactly the same first cycle irreversible capacity (400 mA·h/g). By in situ X-ray diffraction (not shown here), we found that only CoO is recovered at the top of the first charge for both cells, revealing that bypassing the first texturing discharge step has no positive impact on the extent of the back formation of the oxide. This point rules out any drastic implication of the first formatting cycle into this systematic drawback, and other mechanisms have to be put forward and/or found to explain and solve this point, essential to reach competitive performances for conversion reactions.

Conclusions

In the present work, spinel cobalt oxide has been successfully obtained via a one-step precipitation process through oxidation of Co^{2+} in alkaline aqueous solution at 100 °C and optimized washing of the precipitate by acidic solution to remove byproducts. The as-prepared product is made of micrometric porous agglomerates (230 m^2/g, 42% porous volume) consisting of 4 nm crystallized particles and of narrow pore size distribution around 4 nm as well. This texture causes a drastic improvement in reversibility when compared to isolated particles of the same size or even for smaller agglomerates. This shows that pristine and extremely small particles with high specific surface areas can react with lithium at very low voltages, at least for 15 cycles, stressing the major role played by the textural organization onto the cycle life of small domains. The finding of the drastic negative effect of the grinding onto these performances is not to be neglected because it suggests that bad electrochemical results obtained on small particles can also originate from poor electrode making. To some extent, this point could trigger a re-examination of some nanomaterials so far disregarded as the anode for Li-ion batteries.

One of the recurrent main drawbacks of these conversion reactions lies in their irreversible capacity loss. Among other causes, this was attributed to the important modification of the particle texture from bulk to agglomerated nanosized domains occurring during the first "formatting" cycle. The present data obtained on preformatted materials tend to discard this explanation and therefore suggest another origin of this initial loss. Bypassing this formatting is found to have no effect on the back formation of the oxide upon charging the cell, always found limited to the formation of CoO instead of Co_3O_4. Extended cycling comes with a progressive capacity fading that we could correlate with oxide dissolution in the battery electrolyte. This prompted the present investigations dealing, on one hand, with coating of our agglomerates to prevent or limit this dissolution, and on the other hand, with understanding its dissolution process.

The postannealing of these powders induces major modifications of their packing and internal organization, not only as a result of the sintering and grain growth but also because of the loss of over-heated trapped water. This emphasizes that even the drying of these powders has to be carefully performed if their maximal compaction and pristine texture are to be maintained.

Acknowledgment. The authors thank Lydia Laffont (LRCS) for TEM pictures, M. Schindler (Netzsch) and Karim Djellab (LRCS) for mass spectrometer analysis, and Francesc Mestre (Institut de Ciència de Materials de Barcelona) for TGA analysis under H_2. The authors also want to deeply thank P. Poizot (LRCS), C. Masquelier (LRCS), M.R. Palacín, and M. Casas (Institut de Ciència de Materials de Barcelona) for helpful discussions and sharing their knowledge.

CM070048C